Graphical Abstract

Hysteresis Compensation in Temperature Response of Fiber Bragg Grating Thermometers Using Dynamic Regression

Zeeshan Ahmed

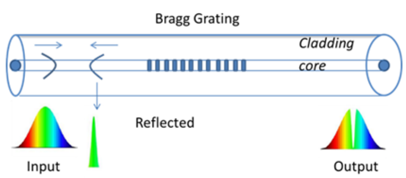

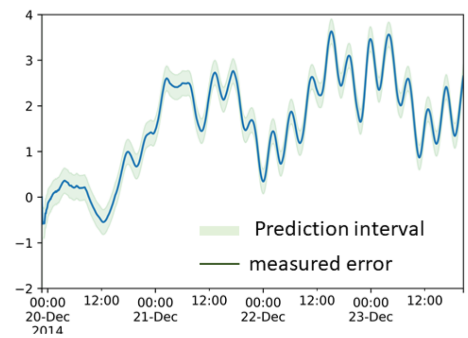

Highlights

Hysteresis Compensation in Temperature Response of Fiber Bragg Grating Thermometers Using Dynamic Regression

Zeeshan Ahmed

- We demonstrate incorporation of device physics-knowledge into building of interpretable machine learning models for photonic thermometers
- Application of Autoregressive Integrative Moving Average (ARIMA) models reduce measurement uncertainties by $\approx 70\%$

Hysteresis Compensation in Temperature Response of Fiber Bragg Grating Thermometers Using Dynamic Regression

Zeeshan Ahmed[a]

[a]*National Institute of Standards and Technology, Physical Measurement Laboratory, Sensor Science Division, 100 Bureau Drive, Gaithersburg, 20899, MD, USA*

Abstract

In recent years there has been considerable interest in using photonic thermometers such as Fiber Bragg grating (FBG) and silicon ring resonators as an alternative technology to resistance-based legacy thermometers. Although FBG thermometers have been commercially available for decades their metrological performance remains poorly understood, hindered in part by complex behavior at elevated temperatures. In this study we systematically examine the temporal evolution of the temperature response of 14 sensors that were repeatedly cycled between 233 K and 393 K. Data exploration and modelling indicate the need to account for serial-correlation in model selection. Utilizing the coupled-mode theory treatment of FBG to guide feature selection we evaluate various calibration models. Our results indicates that a dynamic regression model can effectively reduce measurement uncertainty due to hysteresis by up to $\approx 70\%$.

Keywords: Photonic thermometry, hysteresis compensation, ARIMA, Couple-mode Theory, Machine Learning, Fiber Bragg gratings
PACS: 0000, 1111
2000 MSC: 0000, 1111

---

1. Introduction

Temperature measurements encompass almost every aspect of modern life ranging from advanced manufacturing to health screening constituting a multi-billion-dollar enterprise that is expected to continue growing as the use of temperature sensors proliferate [1] (and refs within). Many thermometry techniques have been developed to meet the varied needs of the user community including resistance-based devices, such as thermistors and platinum resistance thermometers, as well as other sensing modalities including thermocouples, diodes and florescent probes. Standardized manufacturing of metal and semi-conductor based devices ensures an acceptable uncertainty (100 mK to few kelvin) over a given temperature range using nominal coefficients. Tighter uncertainty performance (< 100 mK) requires time consuming calibrations of each individual sensor [2, 3, 4].

The size of the temperature sensor market is a powerful motivator for developing novel technologies targeted towards meeting present and future measurement needs. The existing metrology infrastructure and user expectations of minimum uncertainty metrics along with C-SWaP (cost, size, weight and power) performance requirements represent a formidable barrier to wide-spread adoption of any new temperature measurement technology [5]. As such, any emerging technology is expected to not only provide a novel utility but be backwards compatible with existing infrastructure. Photonic thermometers due to their small size, excellent thermal conductivity and compatibility with telecom infrastructure are expected to meet or exceed user demands[5]. In recent years the photonic thermometry community has largely focused on exploration of novel materials (e.g. silicon[1, 6, 7, 8], silicon nitride[9], diamond, etc[10]), device configurations (Bragg waveguides[11], ring resonators[1, 6], photonic crystal cavities[12] etc) and instrumentation to widen the application window of photonic thermometers beyond metrology labs[6]. Until recently, systematic examination of temperature response of these devices including detailed characterization of measurement uncertainties has been lacking. Several authors have examined the behavior of type-I and type-II fiber Bragg gratings (FBG)[1] sensors at high temperatures and found that the sensors undergo significant hysteresis that is dependent upon both temperature and duration of excursion [13, 14, 15]. These results are broadly in agreement with earlier research on FBG fabrication processes that suggests the fabrication process creates shallow trap states in the bandgap that are "erased" at temperatures higher than 450 K[16, 17, 18, 19]. In ad-

[1]grating types refer to photo-sensitivity mechanism used in writing of the grating. Type 1 rely on UV inscription in photosensitive fibers while Type II gratings are written using localized "damage" caused by two photon absorption

dition, thermally driven ion migration between the fiber core and cladding, glass transition driven stress-strain changes in the fiber, crystallization of α-quartz phase, grating erasure at elevated temperatures and mode mixing are suspected to contribute to measurement uncertainty[17, 18]. At temperatures below 450 K, mechanistic details of thermal hysteresis are unknown[16, 20]. Understanding the mechanism responsible for the hysteresis and quantifying its time-dependent impact on measurement uncertainties are the next steps in the development of FBG thermometers. In this study, we take a physics-informed approach to modeling hysteresis induced changes in the temperature response of FBG sensor. We rely on methods of machine learning and time series forecasting to develop a practical model that can be cost-effectively deployed in industrial setting. We note that elucidation of mechanistic details of hysteresis process i.e. specific changes to the chemical potential or bandgap of the sensor is beyond scope of this study.

2. Experimental

In this study we have utilized commercially available FBG acquired from five different vendors. One set of sensor were coated with a protective layer of polyimide while another set of sensors were coated with an acrylic layer. All other sensors were acquired without the polymeric coating. The fibers were stored in a humidity controlled environment (20% Relative Humidity) prior to use. Each fiber was cleaved such as to leave 2 mm of excess fiber on one side of the sensor, with the other side, 0.5 m long, terminated in a fiber optic coupler. Unless noted otherwise, the sensor was then guided through a T-coupler into a glass tube. The active sensing area of the sensor, at the bottom of the glass tube, was placed inside a through-hole opening (200 μm dia.) of a small copper cylinder. The copper housing provides a strain-free mechanism for anchoring the loose fiber end whilst simultaneously providing a large thermal mass to ensure the the sensor remains in steady equilibrium. The glass tube was then continuously flushed with free-flowing Ar gas to prevent moisture condensation at temperatures below 283 K.

The interrogation system has been described in detail elsewhere[13]. Briefly, the assembled FBG thermometer was placed in a cylindrical Aluminum block (25 mm diameter, 170 mm length). The cylinder has two 150 mm long blind holes (2.5 mm and 6.5 mm diameter) for accommodating a calibrated thermister or platinum resistance thermometer and the assembled FBG sensor, respectively. The calibrated thermometer's uncertainties over the temperature range of 233 K to 393 K are below 10 mK. The Aluminum block is placed inside the dry-well calibrator (Fluke 9170) whose temperature is controlled by software written in LabVIEW that cycles the temperature between 233 K to 393 K at preset intervals intervals (typically 5 K). Once the set temperature is achieved, the program allows for an equalisation period (20 mins unless noted otherwise). Following the equalization period the laser (New Focus TLB-6700[2]) is scanned over a ≤ 2 nm window around the Bragg reflection peak. A small amount of laser power was immediately picked up from the laser output for wavelength monitoring (HighFinesse WS/7) while the rest, after passing through the photonic device via an optical circulator (ThorLabs CIR1550PM-FC), was detected by a large sensing-area power meter (Newport, model 1936-R). Consecutive scans were recorded at each temperature and each sensor was thermally cycled at least three times in each run unless noted otherwise. The recorded data was fitted using a cubic spline to extract peak center, peak height, and peak width as a function of temperature. The assembled dataset contains temperature response of 22 sensors including three quarter-phase gratings and two regenerated-FBG. The r-FBG's response is not included in the analysis presented below. Six other sensors were eliminated from final consideration due to insufficient number of thermal cycles (one or less cycles were successfully collected). Features recorded against temperature include date and time of the measurement, peak center, peak height, full width at half max, area, kurtosis, sensor/grating type, coating, vendor (composite variable standing in for fabrication process variability), time, laser power and experiment type (experiments where number of consecutive scans is 100 or greater are referred to "annealing" as these experiments were designed to detect any slow relaxation process that might be occurring following temperature step). Data exploration was carried out using standard python[21] libraries (pandas[22], seaborn[23], matplotlib[24]) while sklearn sci-kit[25] and statmodels[26] libraries were used for data modeling. A brief discussion of the exploratory data analysis and methodology employed for data modeling is included in the supplemental.

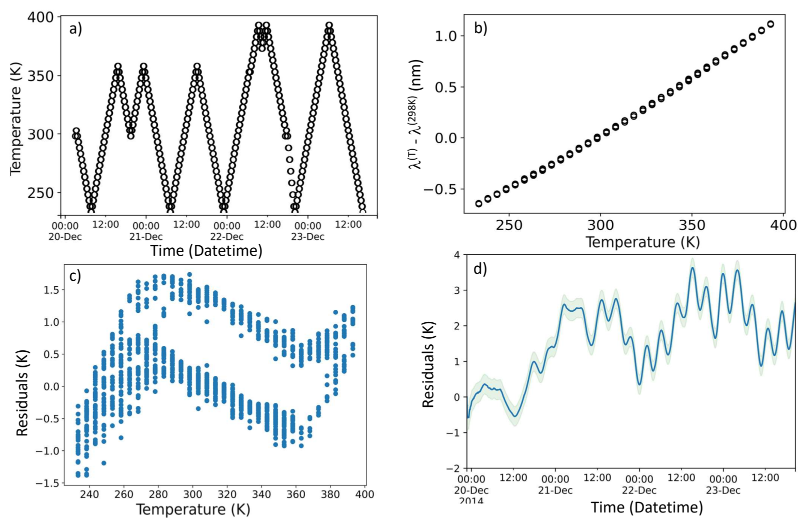

Figure 1: a) Measured temperature cycling profile for sensor S3. b) Measured wavelength detunning vs temperature shows strong quasi-linear dependence that can be modeled as a quadratic function. c) residual of a quadratic fit shows significant departures from normal distribution due to hysteresis. d) time dependence of the residuals from the quadractic fit shown in solid line clearly exhibits a linear increasing trend. The shaded region marks the confidence interval for one-step prediction of AutoRegressive Integrated Moving Average (ARIMA) models trained on the calibration ramp (see discussion for details.

3. Results and Discussion

We explored the complete dataset for possible correlations between temperature and sensor features (see supplemental for details). Exploratory data analysis indicates that besides peak center, which is strongly correlated with temperature, a multitude of features show some degree of correlation with temperature and could be useful in constructing a temperature inference model. Using all of these features together, however would be imprudent. To whittle down the number of candidate features we note that the temperature response of the FBG (and any photonic thermometer in general) relies on the thermo-optic coefficient to transduce temperature changes into the frequency changes[5] (and references within). We therefore, use coupled-model theory treatment of FBG[27, 17, 20] to narrow our feature selection down to only those features that are dependent on the grating refractive index.

The refractive index of the grating can be written as[17]:

$$n = n_{\text{eff}}^{o} + \Delta n_{\text{eff}}^{\text{mean}} + \Delta n_{\text{eff}}^{\text{mod}} cos(\frac{2\pi z}{\Lambda}) \tag{1}$$

where n_{eff}^{o} is the effective index of the unperturbed fiber, $\Delta n_{\text{eff}}^{\text{mean}}$ and $\Delta n_{\text{eff}}^{\text{mod}}$ are the "DC" (period-average) and "AC" (sinusodal change over the period) components of the effective index, respectively[17, 27]. The AC component can be evaluated by examining the maximum reflectivity ($\Delta n_{\text{eff}}^{\text{mod}} = \frac{\lambda_B \tanh^{-1}(\sqrt{(R_{\max})}}{\pi l}$) or in the case of highly reflective gratings where reflectance does not appear to be a sensitive measure of $\Delta n_{\text{eff}}^{\text{mod}}$, FWHM of the grating spectra can be used. The FWHM of the grating response is known to vary linearly with changes in index modulation. The DC component of the refractive index change of a grating is given by $\Delta n_{\text{eff}}^{\text{mean}} = \frac{\Delta\lambda_B}{2\Lambda}$ and can be measured by tracking the detunning of the grating center wavelength away from the designed wavelength[17, 27, 16].

We therefore restrict ourselves to core group of endogenous variables derived from spectral features- peak center, maximum reflectance, FWHM and kurtosis (stand-in for systematic variations in index along the grating length) to construct potential models. As a baseline model we use simple linear regression between $(\lambda_B - \lambda_B^{(298\text{ K})})$ and temperature as a quadratic function

[2]Any mention of commercial products is for informational purposes only; it does not imply recommendation or endorsement by NIST.

(Table 1).[3] We designate the first ascending ramp as the calibration run treating it as our training data upon which the regression model is trained. The remaining data is used as "out-of-sample" validation set to not only evaluate how well the trained model generalizes the sensor response but also to characterize and quantify the impact of thermally induced hysteresis. The baseline model indicates an average training error of 513 mK and out-of sample error of 878 mK. Ten of the 14 sensors examined here show significant thermal hysteresis or ageing effects (training error= 461 mK and out-of-sample error = 1040 mK). In these sensors hysteresis appears to be additive resulting in an offset error that shifts the intercept indicating the overall n_{eff} is increasing as the sensor is exposed to elevated temperature (Fig 1).

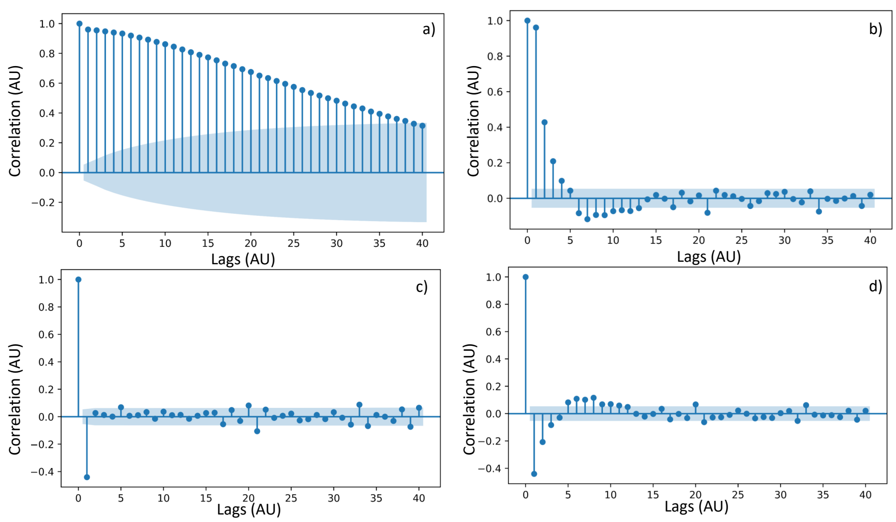

Figure 2: Autocorrelation function (ACF) of S3 sensor's residual is plotted against computed time lags (a) and first-differenced residuals (c) are shown. b and d). Similarly on the right hand panel the partial-autocorrelation function (PACF) plot for S3 sensor's residual (b) and first-differenced residuals (d) are shown. The shaded region marks the uncertainty interval for the auto-correlation coefficients. These plots indicate that hysteresis in S3 is can be modeled as (1,1, [1,2,4,5]) process. See supplemental for ACF and PACF plots for every sensor examined in this study.

To improve upon our baseline model's performance we need to account for changes in n_{eff} as the sensor is being thermally cycled. Equation 1 pro-

[3] We used detuning as the independent parameter since it shows stronger correlation with temperature than peak center. See supplemental for details

vides a framework for breaking down changes in n_{eff} as arising from the AC or DC components of the grating. As noted above the aging effects result in redshift away from the grating wavelength at the start of thermal cycling, behaving as a DC refractive index change process. We model this redshift in baseline grating wavelength by employing a dynamic regression[28] model where the residuals from the training model are used to train a Autoregressive Integrated Moving Average (ARIMA)[28] whose output is added to training /calibration model's output. We examined the auto correlation and partial auto-correlation plots of the residuals to determine a range of (p, d, q)[4] parameters for the ARIMA model that are needed to describe the time dependent behavior of the residuals (Fig 2). As shown in Fig 1d the time evolution of residuals is a non-stationary process as indicated by increasing trend. The presence of this trend is also captured by the ACF plot (Fig 2a) which shows positive values for the auto-correlation coefficient that slowly decrease as lags increase. In contrast, the first differenced residual time series' ACF plot is dominated by the first time lag indicating the time series can be transformed into a stationary process by taking the first difference. Furthermore, we note that a lack of significant peaks at longer time lags or multiples of time lags indicates a lack of cyclical behavior in the time evolution of the hysteresis.

The ACF and PACF plots of the difference residuals are used to determine the dominant terms for the autoregressive and moving average terms by selecting the highest time time lags correlation coefficients significantly larger than the calculated uncertainty. These parameters were then further optimized by maximizing the log-likelihood of the fit. Overall our exploration of parameter space indicates that simple ARIMA models containing a linear trend ($d = 1$) and short term moving average ($q < 10$) and autoregressive term ($p < 2$) is sufficient to capture long term changes in the residual across all sensors. That is, the long-term drift in FBG can be described as consisting of three components: a slow linear drift, a short-term memory (< 300 s) and a white noise component. Caution should be exercised when using the order of ARIMA terms to draw insights into physical processes responsible for the observed hysteresis. Given that changes in Bragg wavelength are due to changes in the n_{eff}, we interpret the linear trend as indicating the n_{eff}

[4] p, d, q refer to the order of autoregressive, integrative and moving average processes. Hence a (1,1,1) process would be a described as being autoregressive in the first order with a simple linear trend and a moving average of one. The first order difference i.e. linear trend correction is necessary to make the time series stationary

of the sensor shows a slow, linear increase as thermal cycles progress. The origin(s) of the short-term memory effect is difficult to assign. It is likely that this term is capturing short term process such as modal noise due to thermal or strain relaxation in the fiber or short-term correlation in the temperature control loop of the bath.

As shown in Table 1 the mean uncertainty for one-step prediction is only 265 mK while uncertainty when using dynamic prediction[5] over the out-of-sample set is 623 mK which is 69% and 41% lower than the baseline model, respectively. We note that while the model performs well over the short-term (one-step forecast), uncertainty in the forecast grows with the horizon. As such these models are most appropriate over finite horizons. For metrology problems requiring infinite horizons, state-space models or long-short term memory (LSTM) models[29] that incorporate device physics, chemistry and thermal history may be more appropriate.

We evaluated the possibility that hysteresis maybe accounted by changes in the AC component i.e. the observed hysteresis may derive in part from the grating contrast erasure. As noted above, changes in the AC component of index proportionally impact the amplitude and width of the resonance spectra. In order to incorporate the AC index change into our model, we therefore incorporate additional features (time normalized amplitude, fractional FWHM and kurtosis)[6] into a multivariate regression model employing L2 regularization ($\alpha = 0.000001$), multi-layer preceptrons (MLP) with one or two hidden layers employing sigmodial activation ([100x1] or [5x1],[3x1] , respectively) and a hidden-state-like model where amplitude, fractional width and kurtosis are transformed and regressed to predict peak center detunning, $(\lambda_B - \lambda_B^{(298K)})$, which in turn is added as a feature along with measured peak center detunning to a multivariate regression model. As shown in Table 2 the resulting models fail to improve upon the baseline model, generally performing worse. Failure of these models to accurately compensate for hysteresis suggests that while spectral features other than the peak center show temporal changes, these changes are neither linearly correlated with temperature nor the observed peak center. Hysteresis in FBG can be adequately modeled

[5]see supplemental for discussion of differences between one-step vs dynamic prediction

[6]kurtosis is a stand-in variable for non-uniform changes in AC index along the fiber axis i.e. it reports on the dephasing of the grating index contrast. time-normalized amplitude and fractional width are used in place of amplitude and FWHM, respectively, because they show stronger correlations with peak center.

as a DC-only process.

Table 1: Results of Dynamic Regression Model for Hysteresis Compensation

Sensor	Hysteric	Training error	Out of sample error	One step error	Dynamic pred. error	Uncorrected error over dynamic range
S1	Yes	0.1369	2.106	0.32	0.79	1.9
S2	Yes	0.352	1.553	0.09	0.78	1.45
S3	Yes	0.4683	1.06	0.15	0.42	0.69
S4	Yes	0.774	0.88	0.34	0.48	0.81
S5	Yes	0.4576	0.761	0.17	0.42	0.598
S6	Yes	0.2485	0.749	0.25	0.6	0.67
S7	Yes	0.5381	0.808	0.34	0.55	2.35
S8	Yes	0.8184	1.269	0.63	1.05	1.08
S9	Yes	0.4565	0.81	0.15	0.73	0.54
S10	Yes	0.3622	0.4	0.21	0.41	0.41
S11	No	0.7529	0.6985	0.29	0.47	0.73
S12	No	0.5255	0.5745	0.16	0.6	0.66
S13 [a]	No	0.445	0.447	0.29	0.48	0.45
S13 [b]	No	0.424	0.431	0.28	0.57	0.43
S14	No	0.9336	0.6275	0.25	0.85	0.83
Mean [c]		0.461	1.04	0.265	0.623	1.05
Mean [d]		0.513	0.878	0.261	0.613	0.9

[a] input power less than 10 microwatt
[b] input power 2.5 mW
[c] mean of hysteretic sensors only
[d] mean of all sensors

Table 2: Modeling Hysteresis using an Expanded set of Spectral Features as Inputs to the Calibration Model

Model	Training Error (K)	Out of Sample Error (K)
Baseline[a]	0.513	0.878
Hidden-state-like[b]	0.627	6.66
Lasso [c]	1.13	6.31
MLP[d]	10.42	22.98
MLP [e]	7.88	21.14

[a] peak center detuning is the only input

[b] fractional width, kurtosis and amplitude are used to predict wavelength detunning. this prediction is used as an input to a regression model along with measured wavelength detunning to infer temperature

[c] input features include wavelength detunning, kurtosis, fractional width and area, alpha = 0.000001;

[d] hidden layers [5*3], alpha = 0.0001

[e] hidden layer [100], alpha = 0.0001

4. Summary

Long term hysteresis or ageing effects in photonic thermometers [13, 14, 15, 12] represent a significant measurement science challenge to the adoption of photonic thermometry in-lieu of resistance thermometers. In this study we demonstrate that guided by device physics we can deploy proven statistical techniques to model the ageing effects and successfully reduce the measurement uncertainty by up to 70%. Our work here serves as a motivation to develop first principles based thermo-optic coefficient models that can be co-depolyed with ARIMA models in Kalman filter like predictor-corrector algorithms to reduce measurement uncertainty and gain mechanistic understanding of processes driving long and short term drift in sensor characteristics.

5. Acknowledgments

Author thanks Dan Samarov, Gilad Kusne, Tobias Herman and Tyrus Berry for helpful discussion. This work was funded by NIST-on-a-chip (NOAC) initiative.

6. Disclosures

The author declares no conflicts of interest.

References

[1] H. Xu, M. Hafezi, J. Fan, J. M. Taylor, G. F. Strouse, Z. Ahmed, Ultra-sensitive chip-based photonic temperature sensor using ring resonator structures, Opt. Express 22 (3) (2014) 3098–3104. doi:10.1364/OE.22.003098.
URL `http://opg.optica.org/oe/abstract.cfm?URI=oe-22-3-3098`

[2] H. Preston-Thomas, The international temperature scale of 1990 (its-90), Metrologia 27 (1) (1990) 3–10.

[3] Consultative Committee for Thermometry under the auspices of the International Committee for Weights and Measures, *mise en pratique for the definition of the kelvin in the SI*, `https://www.bipm.org/en/publications/mises-en-pratique` (2019).

[4] B. W. Mangum, G. F. Strouse, W. F. Guthrie, R. Pello, M. Stock, E. Renaot, Y. Hermier, G. Bonnier, P. Marcarino, K. S. Gam, K. H. Kang, Y.-G. Kim, J. V. Nicholas, D. R. White, T. D. Dransfield, Y. Duan, Y. Qu, J. Connolly, R. L. Rusby, J. Gray, G. J. Sutton, D. I. Head, K. D. Hill, A. Steele, K. Nara, E. Tegeler, U. Noatsch, D. Heyer, B. Fellmuth, B. Thiele-Krivoj, S. Duris, A. I. Pokhodun, N. P. Moiseeva, A. G. Ivanova, M. J. de Groot, J. F. Dubbeldam, Summary of comparison of realizations of the ITS-90 over the range 83.8058 k to 933.473 k: CCT key comparison CCT-k3, Metrologia 39 (2) (2002) 179–205. doi:10.1088/0026-1394/39/2/7.
URL `https://doi.org/10.1088/0026-1394/39/2/7`

[5] Z. Ahmed, Role of quantum technologies in reshaping the future of temperature metrology, Measurement: Sensors 18 (2021) 100308. doi:https://doi.org/10.1016/j.measen.2021.100308.
URL `https://www.sciencedirect.com/science/article/pii/S2665917421002713`

[6] R. Eisermann, S. Krenek, G. Winzer, S. Rudtsch, Photonic contact thermometry using silicon ring resonators and tuneable laser-based spectroscopy, tm - Technisches Messen 88 (10) (2021) 640–654. doi:doi:10.1515/teme-2021-0054.
URL `https://doi.org/10.1515/teme-2021-0054`

[7] S. Janz, R. Cheriton, D.-X. Xu, A. Densmore, S. Dedyulin, A. Todd, J. H. Schmid, P. Cheben, M. Vachon, M. K. Dezfouli, D. Melati, Photonic temperature and wavelength metrology by spectral pattern recognition, Opt. Express 28 (12) (2020) 17409–17423. doi:10.1364/OE.394642.
URL `http://opg.optica.org/oe/abstract.cfm?URI=oe-28-12-17409`

[8] C. Zhang, G. Kang, Y. Xiong, T. Xu, L. Gu, X. Gan, Y. Pan, J. Qu, Photonic thermometer with a sub-millikelvin resolution and broad temperature range by waveguide-microring fano resonance, Opt. Express 28 (9) (2020) 12599–12608. doi:10.1364/OE.390966.
URL `http://opg.optica.org/oe/abstract.cfm?URI=oe-28-9-12599`

[9] C. Zhang, G.-G. Kang, J. Wang, S. Wan, C.-H. Dong, Y.-J. Pan, J.-F. Qu, Photonic thermometer by silicon nitride microring resonator with milli-kelvin self-heating effect, Measurement 188 (2022) 110494.

doi:https://doi.org/10.1016/j.measurement.2021.110494.
URL https://www.sciencedirect.com/science/article/pii/S0263224121013774

[10] J. A. Smith, P. Hill, C. Klitis, M. Sorel, P. A. Postigo, L. Weituschat, M. D. Dawson, M. J. Strain, High precision diamond-on-gan photonic thermometry enabled by transfer printing integration, in: OSA Advanced Photonics Congress 2021, Optica Publishing Group, 2021, p. IM1A.4. doi:10.1364/IPRSN.2021.IM1A.4.
URL http://opg.optica.org/abstract.cfm?URI=IPRSN-2021-IM1A.4

[11] N. N. Klimov, S. Mittal, M. Berger, Z. Ahmed, On-chip silicon waveguide bragg grating photonic temperature sensor, Opt. Lett. 40 (17) (2015) 3934–3936. doi:10.1364/OL.40.003934.
URL http://opg.optica.org/ol/abstract.cfm?URI=ol-40-17-3934

[12] N. Klimov, T. Purdy, Z. Ahmed, Towards replacing resistance thermometry with photonic thermometry, Sensors and Actuators A: Physical 269 (2018) 308–312. doi:https://doi.org/10.1016/j.sna.2017.11.055.
URL https://www.sciencedirect.com/science/article/pii/S0924424717318940

[13] Z. Ahmed, J. Filla, W. Guthrie, J. Quintavalle, Fiber bragg grating based thermometry, NCSLI Measure 10 (4) (2015) 28–31. doi:10.1080/19315775.2015.11721744.

[14] D. Grobnic, C. Hnatovsky, S. Dedyulin, R. B. Walker, H. Ding, S. J. Mihailov, Fiber bragg grating wavelength drift in long-term high temperature annealing, Sensors 21 (4) (2021). doi:10.3390/s21041454.
URL https://www.mdpi.com/1424-8220/21/4/1454

[15] R. Eisermann, S. Krenek, T. Habisreuther, P. Ederer, S. Simonsen, H. Mathisen, T. Elsmann, F. Edler, D. Schmid, A. Lorenz, A. A. F. Olsen, Metrological characterization of a high-temperature hybrid sensor using thermal radiation and calibrated sapphire fiber bragg grating for process monitoring in harsh environments, Sensors 22 (3) (2022). doi:10.3390/s22031034.
URL https://www.mdpi.com/1424-8220/22/3/1034

[16] T. Erdogan, V. Mizrahi, P. J. Lemaire, D. Monroe, Decay of ultraviolet-induced fiber bragg gratings, Journal of Applied Physics 76 (1) (1994)

73–80. arXiv:https://doi.org/10.1063/1.357062, doi:10.1063/1.357062. URL https://doi.org/10.1063/1.357062

[17] H. Patrick, S. L. Gilbert, A. Lidgard, M. D. Gallagher, Annealing of bragg gratings in hydrogen-loaded optical fiber, Journal of Applied Physics 78 (5) (1995) 2940–2945. arXiv:https://doi.org/10.1063/1.360753, doi:10.1063/1.360753. URL https://doi.org/10.1063/1.360753

[18] D. P. Hawn, The effects of high temperature and nuclear radiation on the optical transmission of silica optical fibers, Ph.D. thesis, The Ohio State University (2012).

[19] A. Munko, S. Varzhel', S. Arkhipov, A. Gribaev, K. Konnov, M. Belikin, The study of the thermal annealing of the bragg gratings induced in the hydrogenated birefringent optical fiber with an elliptical stress cladding, Journal of Physics: Conference Series 735 (2016) 012015. doi:10.1088/1742-6596/735/1/012015. URL https://doi.org/10.1088/1742-6596/735/1/012015

[20] S. Pal, J. Mandal, T. Sun, K. T. V. Grattan, Analysis of thermal decay and prediction of operational lifetime for a type i boron-germanium codoped fiber bragg grating, Appl. Opt. 42 (12) (2003) 2188–2197. doi:10.1364/AO.42.002188. URL http://opg.optica.org/ao/abstract.cfm?URI=ao-42-12-2188

[21] G. Van Rossum, F. L. Drake, Python 3 Reference Manual, CreateSpace, Scotts Valley, CA, 2009.

[22] Wes McKinney, Data Structures for Statistical Computing in Python, in: Stéfan van der Walt, Jarrod Millman (Eds.), Proceedings of the 9th Python in Science Conference, 2010, pp. 56 – 61. doi:10.25080/Majora-92bf1922-00a.

[23] M. L. Waskom, seaborn: statistical data visualization, Journal of Open Source Software 6 (60) (2021) 3021. doi:10.21105/joss.03021. URL https://doi.org/10.21105/joss.03021

[24] J. D. Hunter, Matplotlib: A 2d graphics environment, Computing in Science & Engineering 9 (3) (2007) 90–95. doi:10.1109/MCSE.2007.55.

[25] F. Pedregosa, G. Varoquaux, A. Gramfort, V. Michel, B. Thirion, O. Grisel, M. Blondel, P. Prettenhofer, R. Weiss, V. Dubourg, J. Vanderplas, A. Passos, D. Cournapeau, M. Brucher, M. Perrot, E. Duchesnay, Scikit-learn: Machine learning in Python, Journal of Machine Learning Research 12 (2011) 2825–2830.

[26] S. Seabold, J. Perktold, statsmodels: Econometric and statistical modeling with python, in: 9th Python in Science Conference, 2010, pp. 92–96.

[27] T. Erdogan, Fiber grating spectra, Journal of Lightwave Technology 15 (8) (1997) 1277–1294. doi:10.1109/50.618322.

[28] R. J. Hyndman, G. Athanasopoulos, Forecasting:Principles and Practice, 2nd edition, OTexts, Melbourne, Australia, 2018.

[29] S. Hochreiter, J. Schmidhuber, Long Short-Term Memory, Neural Computation 9 (8) (1997) 1735–1780. arXiv:https://direct.mit.edu/neco/article-pdf/9/8/1735/813796/neco.1997.9.8.1735.pdf, doi:10.1162/neco.1997.9.8.1735.
URL https://doi.org/10.1162/neco.1997.9.8.1735